JOURNAL OF MATERIALS SCIENCES 33 (1998) 2339–2355

Kinetics of direct nitridation of pelletized silicon grains in a fluidized bed: experiment, mechanism and modelling

Z. R. JOVANOVIC*
Department of Chemical Engineering, Oregon State University, Corvallis, OR 97331, USA
E-mail: zjovanovic@dow.com

A fluidized-bed nitridation of pelletized silicon grains having a wide size distribution was carried out in the temperature range 1200–1300 °C under conditions free of external heat and mass transfer effects. N_2(30%–90%)–H_2(5%–50%)–Ar (balance) mixtures were used as the nitriding gas at atmospheric pressure. Both the yield of α-Si_3N_4 and the final overall conversion of silicon are affected by temperature and nitrogen gas concentration in a nitriding atmosphere, but hydrogen gas has a minor effect on either of these. After accounting for some of the structural changes that occur during nitridation, a simple model was derived. The model has shown that the pseudo-asymptotic exponential conversion trend in the second nitridation stage could be explained by various reaction mechanisms, adjusted for properties of the size distribution of silicon grains and the experimentally observed spalling of the product scale from the silicon surface. In the investigated range of experimental conditions, nitridation could be considered as having an apparent activation energy of $E_{app} \approx 340$ kJ mol^{-1}. © *1998 Chapman & Hall*

1. Introduction

In the last decade, silicon nitride (Si_3N_4) has become an attractive ceramic for making components that operate under severe mechanical and thermal stresses. This material exists as amorphous, or in two crystalline modifications, designated α and β. Because of its toughness and excellent resistance to thermal shock and oxidation, the more desirable polymorph for high-temperature engineering applications is the β-Si_3N_4 [1]. Fabricating good-quality β-Si_3N_4 parts is, however, a complex multi-step process. The starting raw material is a fine Si_3N_4 powder, mixed with special additives (Al_2O_3–Y_2O_3) and shaped into a desired component. Finally, the component is sintered at high temperatures (1600–1750 °C) where the structural densification occurs, providing a micro-structure of high mechanical and thermal strength.

The chemical and physical properties of the starting Si_3N_4 powder are critical to success in both fabricating a dense part and ensuring the required physical properties of the component. The major properties of the starting powder that are relevant to the quality of the final part are α/β phase ratio, trace impurities, and size distribution of crystallites and/or agglomerates [2–4]. Despite advances that have been made in sintering essentially pure β-form [5, 6], the facts (i) that the α to β phase transformation during the final sintering step plays an important role in the densification process, and (ii) that the α-form dissolves faster in the sintering additives than does the β-form, make it preferable to use a high α-phase content Si_3N_4 as the starting raw powder. This also enables milder sintering conditions (atmospheric pressure and lower temperatures). Some small amount of the β-form still present in the starting material has been proved useful in providing nucleating sites for the α to β recrystallization during the sintering [2]. On the other hand, the presence of metallic impurities (calcium, iron, nickel, chromium) and/or coarser crystallites in the starting powder can lead to severe degradation in strength and catastrophic failures at high temperatures [2]. Therefore, the desired product in the production of raw Si_3N_4 is a sub-micrometre powder with an α/β ratio as high as possible and with strictly controlled contents of the metallic trace impurities. Such a material is commercially produced by thermal decomposition of silicon diiamide [3, 7] and by direct nitridation of silicon [2, 8].

In spite of the outstanding thermo-mechanical properties of Si_3N_4 parts, wide use of this material is constrained partly by its current production cost. This work presents a phase of research dedicated to the

* *Present address*: The Dow Chemical Company, Ceramics and Advanced Materials Research, 52 Building, Midland, MI 48667, USA.

development of a potentially new low-cost direct nitridation process, based on utilizing fluidized-bed technology. Although the handling of fine cohesive powders presents a significant problem in operating fluidized beds [9], this technology offers many advantages for gas–solid reactions [10]. The feature that makes a fluidized-bed reactor particularly attractive for application in a highly exothermic process such as direct nitridation of silicon, is a good mixing of solids, reflected by a high heat-transfer efficiency and uniform temperature distribution within the bed.

Proper design of a fluidized-bed reactor must be based on reliable kinetic data. Results of kinetic nitridation studies reported in the literature, however, appear to be applicable only to the specific set of experimental conditions under which the data were obtained. Most of the reported kinetic data were obtained by thermo-gravimetric analysis (TGA), where heat and mass-transfer effects on the overall process rate were often neglected. In addition, much of the variation in those data can be attributed to the effects of a raw silicon grain shape and size distribution. Reported fludized-bed nitridation results [11–13] were obtained in continuously operating fluidized beds, utilizing a significant fraction of inert Si_3N_4 added to the raw silicon material to make temperature control feasible. For this reason, neither these results could provide detailed information about nitridation kinetics. The objectives of this study were to present reliable and scale-insensitive kinetic data for nitridation of a suitable raw silicon precursor as a function of temperature and nitriding atmosphere, and to discuss possible kinetic mechanisms of the nitridation process.

2. Direct nitridation of silicon

Direct nitridation of silicon is the process which accounts for most of the commercially produced Si_3N_4 [2]. Although in some cases NH_3 has been used as the nitrogen source [3, 12], the direct nitridation process is usually based on contacting elemental silicon powder with nitrogen gas at temperatures between 1200 and 1400 °C according to the overall stoichiometric equation

$$N_{2(g)} + 1.5\ Si_{(s)} \rightarrow 0.5\ Si_3N_4(\alpha, \beta)_{(s)} \qquad (1)$$

Reaction 1 is highly exothermic, releasing approximately 736 kJ (mol Si_3N_4)$^{-1}$ at 1230 °C. In the presence of liquid silicon, complete nitridation becomes virtually impossible [7], hence extreme care must be taken to keep the reaction temperature below the melting point of the silicon powder (1410 °C). Also, the liquid silicon can dissolve α-Si_3N_4, after which the product reprecipitates as the β-form, thereby decreasing the yield of the desired product [14].

Direct nitridation of silicon is, however, much more complicated than Equation 1 implies. The presence of oxygen in the reacting system, either as a trace impurity in the nitriding atmosphere or in the native SiO_2 layer covering the silicon surface, may cause an entirely new set of reactions to occur, with crystalline Si_2N_2O and/or gaseous SiO appearing as the products. The latter has even been postulated to be a key reactant for the formation of Si_3N_4 [15, 16], yielding the α-form via the gas-phase reaction with nitrogen [17]. However, ΔG^0 for the reaction between SiO and nitrogen is large and positive (545 kJ (mol Si_3N_4)$^{-1}$ at 1430 °C), thus an efficient sink of oxygen is required if this reaction is to take place [18]. For this reason, hydrogen gas is commonly added to the nitrogen to control the partial pressure of oxygen, maintain gaseous SiO in the system, and prevent the reoxidation of the silicon surface which hinders nitridation [14, 18–20]. In addition, some researchers have reported that the dilution of nitrogen by hydrogen enhances the final extent of the reaction [20, 22] and increases the α/β ratio in the product [15, 20–22].

Another potential problem for understanding the mechanism of this process is the presence of trace metallic impurities in the raw silicon powder (iron, aluminium, calcium) that may significantly affect the progress of nitridation. Campos-Loriz and Riley [23] have reported that the reaction yielding the β-form takes place predominantly at impurity-rich sites. For example, iron tends to form a low melting point alloy with silicon, which provides a liquid phase that dissolves the α-form and facilitates the growth of the undesired β-form [24]. The presence of liquid also enhances the inter-phase contact, which may explain the catalytic role of iron in increasing both the reaction rate and the final extent of the reaction [16, 25]. However, Pigeon *et al.* [16] have reported that the presence of liquid caused by the formation of low melting point eutectics does not necessarily increase the yield of the β-form, but rather that the formation of the β-form is facilitated by the presence of those impurities that favour generation of atomic nitrogen. Another possible explanation for the effect of iron has been reported by Jennings *et al.* [26] who stated that iron could accelerate the nitridation reaction by participating in the removal of the native SiO_2 layer.

Although there are several scenarios proposed to explain the conversion of silicon grains to Si_3N_4 [24, 27–30], at present there is no general agreement regarding the mechanism and kinetics of this process. Apparently, it is very difficult to elucidate the mechanism of the nitridation reaction, even after disregarding the fact that it might consist of two completely separate paths, each leading to the formation of either α- or β-Si_3N_4 [21, 26]. A rigorous comparison of reported experimental data and proposed kinetic models is obscured by the fact that various investigators used different experimental conditions such as compact size, particle-size distribution, raw silicon purity, and trace gas impurities. Also, a particularly difficult task in understanding the mechanism of this process is to distinguish the intrinsic kinetics from possible structural and morphological changes occurring during nitridation [24, 27, 29, 30]. The fact that consistent variability in the final extent of reaction with experimental conditions [22, 24, 31–33] cannot be explained by chemical equilibrium implies that the structural and morphological factors may have a critical role in the overall nitridation kinetics.

3. Experimental procedure
3.1. Precursor
Although preferable for producing a fine Si_3N_4 powder, the direct fluidization of micrometre-size silicon particles is not feasible. Such silicon particles behave as a difficult to fluidize Geldart C powder [10], even at room temperature [34]. Because inter-particle forces and cohesiveness of particles generally increase with temperature, the raw material particles used in this work were porous silicon pellets similar to that used as the precursor in the fluidized-bed nitridation work of Shimizu *et al.* [12]. These pellets were prepared by mixing fine silicon grains (~ 2 μm diameter) into a thick paste with the aid of a suitable binder such as polyvinyl alcohol. The paste was then extruded into granules of an average sieving size of ~ 400 μm, that were afterwards briefly sintered at 1100–1300 °C into slightly cemented together, but not melted, porous pellets [12]. The contents of trace impurities in the raw material are specified elsewhere [22].

Scanning electron micrographs indicated that the precursor silicon pellets were rather cylindrical [35], hence their mean diameter determined by sieving analysis (~ 400 μm) does not present pertinent information about their real size. On the other hand, a back-scattered electron image (BSE) of a cross-section of a pellet (Fig. 1) indicates that the constituent silicon grains have irregular shape, and a wide multimodal size distribution with a fraction of very large grains or maybe grain clusters. The facts that measured size distributions of the original silicon grains were not reproducible (Fig. 2), and that probably an additional agglomeration of the grains occurred during the preparation of the precursor, hinder a reliable interpretation of the actual grain size in the pellets. It should be noted, however, that the measured specific surface areas of the pellets were in the range 1.7–2 $m^2 g^{-1}$ (BET, Micromeritics ASAP 2000) which is in close agreement with the specific surface areas of the original silicon grains, S_w, estimated from the sedimentation grain sizes (Fig. 2).

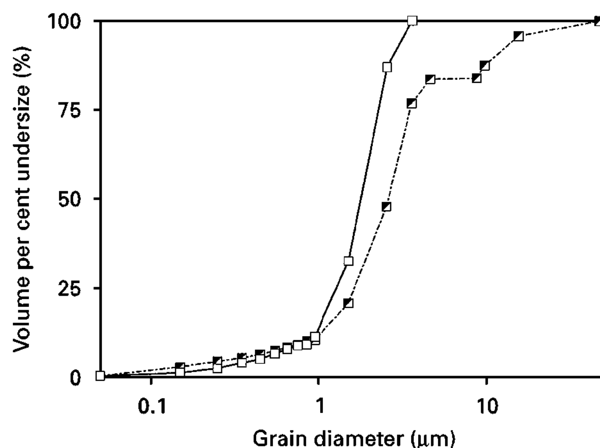

Figure 2 Grain-size distributions, specific surface areas and mean diameters of silicon grains measured prior to pelletization into the precursor (particle sedimentation technique, a Horiba CAPA-700 particle size analyser): (□) *A*, $S_w = 1.899$ $m^2 g^{-1}$, $\bar{d} = 1.33$ μm, (◩) *B*, $S_w = 1.844$ $m^2 g^{-1}$, $\bar{d} = 1.40$ μm.

3.2. Apparatus
Fig. 3 illustrates the experimental apparatus used for studying the kinetics of fluidized-bed nitridation. The apparatus consists of three main units: (i) a mullite fluidized-bed reactor (55 mm diameter, 1200 mm long), situated in a three-heating-zone vertical tube furnace, and equipped with a gas distributor consisting of both a perforated alumina plate and an additional packed bed of coarse alumina beads; (ii) a system for controlling the composition of fluidizing gas mixtures, and (iii) pneumatic solids charge and discharge systems. Flow rates of individual gases (prepurified grade nitrogen, hydrogen, standard grade argon) were measured by calibrated rotameters. The measured oxygen concentrations in the gases were about 5 p.p.m. (Portable Trade Oxygen Analyzer, Teledyne Analytical Instruments Model 311).

Bed temperature was measured with an alumina-shielded R-type thermocouple, inserted into the bed to about 3 cm above the distributor. A pressure transducer (PTD), in conjunction with a data acquisition system (DAS), allowed monitoring of the fluidization regime of the bed by providing on-line measurements of pressure drop through the bed. The reactor pressure was slightly above atmospheric pressure. A detailed description of all of the components of the experimental setup is presented elsewhere [35].

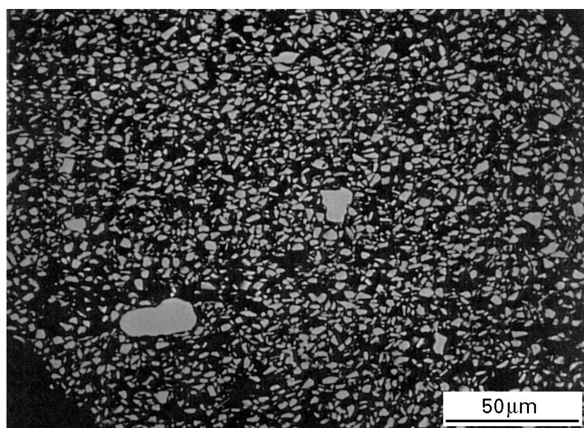

Figure 1 BSE image of a cross-section of a precursor pellet (white, silicon; black, voids) [35].

3.3. Operating fluidizing velocity
The choice of the operating fluidizing gas velocity, u_0, had to be made based on the fact that the density of the pellets increases with the progress of nitridation by approximately a factor of 1.7. In addition, the experiments were to be carried out at various temperatures, and with various hydrogen–nitrogen–argon mixtures having different gas properties. In order to determine a range of u_0 which provides fluidization for the whole range of pellet densities under various properties of gas mixtures, fluidization curves for previously fully nitrided pellets were determined in the temperature range 1200–1350 °C, utilizing hydrogen–nitrogen mixtures with 0–50% H_2 by volume as the fluidizing gas. The results showed that the minimum fluidization velocity of the Si_3N_4 pellets, $u_{mf} \approx 9$ cm s^{-1}, did not

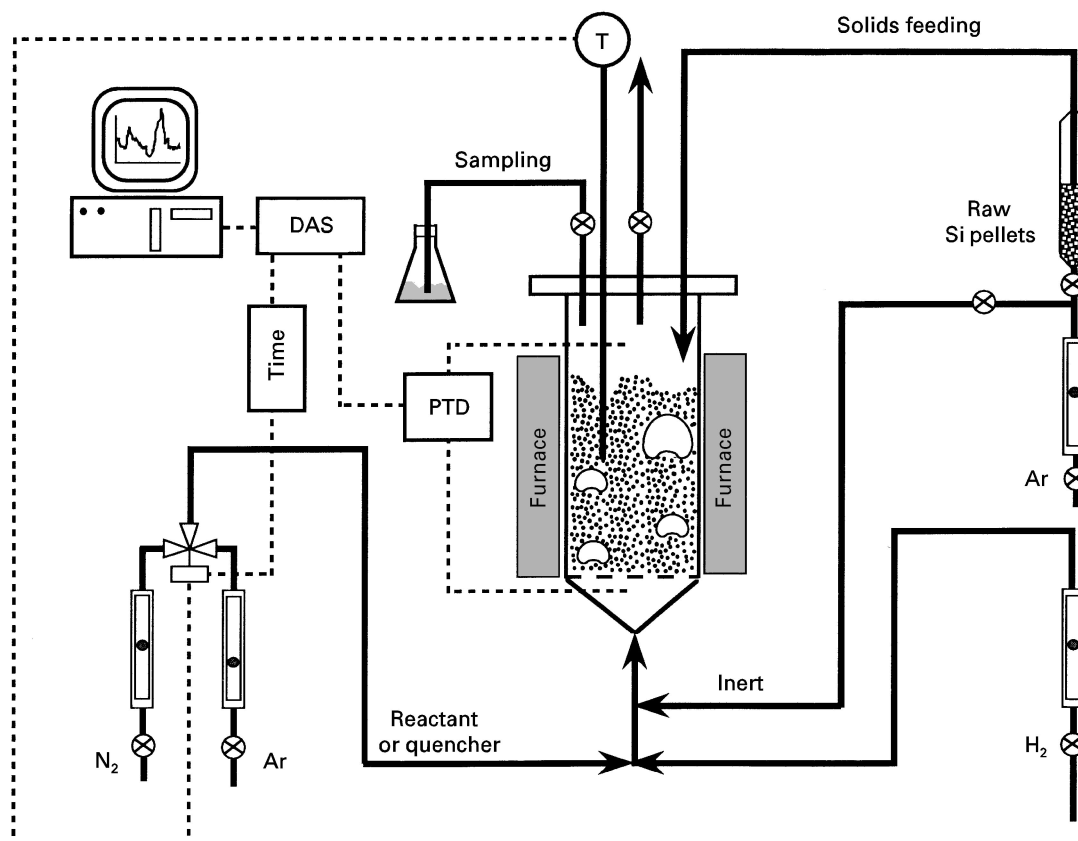

Figure 3 Schematic representation of experimental set-up [35].

vary significantly within a wide range of temperatures and compositions of the fluidizing gas [35]. On the basis of these measurements, u_0 was chosen to be at least 25 cm s^{-1}, which provided vigorously fluidized solids and good fluidization up to 1300 °C. At this and higher operating temperatures, however, u_0 had to be increased to 35 cm s^{-1} in order to prevent agglomeration of the silicon pellets and to ensure stable fluidization conditions.

3.4. Reaction

All the experiments were carried out in batch-solids operations. After the empty reactor was preheated to a prescribed reaction temperature, a 40% H_2–Ar gas mixture was supplied to the bed at a superficial fluidization velocity, u_0, based on the set-point temperature. Silicon pellets (100 g) were first fluidized in the feeding container by argon for approximately 5 min in order to remove the air from the voids, and then charged into the bed by pneumatic transport utilizing argon as the carrier gas. After the bed temperature had reached the set-point (in about 10 min), the pellets were kept fluidized in a 40% H_2–Ar mixture for additional 60 min. This pretreatment was carried out to remove as much of the SiO_2 coating on the silicon surface as possible, i.e. to prepare the precursor for nitridation.

After the precursor was properly treated, the flow rates of hydrogen and argon were readjusted to set the hydrogen concentration at the desired level. The reaction was then initiated by actuating a solenoid valve (5 V d.c.), which switched the feed gas from argon to nitrogen without changing the total volumetric gas flow rate through the bed. As the bed temperature started to rise due to the heat released by nitridation, the bed inventory was quenched by deactivating the solenoid valve, i.e. by switching the feed gas from nitrogen back to argon. It should be noted that the hydrogen feed line was independent and unaffected by an action of the solenoid. The d.c. signal used to actuate the valve also triggered a timer in the data acquisition system, which provided the cumulative reaction and quenching times with a resolution of 1 s. This on/off procedure was implemented only during the very initial stage of nitridation, to control the bed temperature within ± 3 °C of the set-point. At the same time, the set-point on the furnace controller was lowered to adjust the energy input to the furnace until a stable bed operating temperature was achieved without quenching.

The reaction could be terminated (by quenching), and resumed again in seconds (by enabling the nitrogen flow through the bed). The volumetric flow rates of argon (the quencher) and nitrogen (the reactant) were kept the same to maintain the fluidizing velocity at the set point u_0. This was done to compensate for the errors in counting both reaction and quenching times due to the lag time between the action of the solenoid valve and the actual physical appearance of either the quencher or reactant in the bed. In experiments where separate effects of nitrogen and hydrogen concentrations were investigated, an additional argon

line was used to supply inert gas into the bed, and to adjust both nitrogen and hydrogen concentrations to a desired level. At various reaction times, samples of reacted solids (1–3 g) were withdrawn from the reactor through a pneumatic discharge line, without disturbing the reaction conditions in the bed.

The key feature of the experimental setup described above is that it enables a stable isothermal nitridation utilizing an essentially pure silicon precursor, with no inert solids added to act as a heat absorber. In addition, the initial amount of silicon used in this work was much larger than that utilized in the reported TGA experiments, where the limitations in temperature control could cause the difference between the set-point temperature and the actual temperature of a sample to be as high as $\sim 160\,^{\circ}\mathrm{C}$ [33]. According to the faster reaction rate observed in this study, a rough estimate of the temperature gradients in a gas film and within a pellet gives ~ 23 and $\sim 2\,^{\circ}\mathrm{C}$, respectively [35]. Hence, due to the high fluidized solids/immersed bodies heat-transfer coefficient [10], i.e. the fact that the thermocouple actually measured the temperature somewhere in between temperatures of the gas and of the solids, it is believed that the measured bed temperature well represented the pellet temperature. Such temperature control is difficult to achieve in TGA experiments.

3.5. Quantitative analysis of product

The Si/α-/β-Si_3N_4 phase compositions of sample solids were determined by powder X-ray diffraction (XRD). Owing to discrepancies found in the reported methods for determining α-/β-Si_3N_4 ratios and possible effects of preferred orientation and extinction on the determination of Si/α-Si_3N_4 peak ratios, an original method to evaluate calibration constants needed for the quantitative determination of Si/α-/β-Si_3N_4 mixtures has been developed. As described in detail elsewhere [35, 36], the method utilizes unspecified α/β-Si_3N_4 mixtures that are commercially available. The quantitative analysis of the product and the calculation of the silicon conversions (overall and fractional into each of the Si_3N_4 phases) are described elsewhere [22].

4. Results and discussion

A remarkable reproducibility of results and effect of fluidizing velocity on the overall conversion of silicon are demonstrated in Fig. 4. It can be seen that the results of two runs at $1275\,^{\circ}\mathrm{C}$ in a N_2–10% H_2 atmosphere carried out at $u_0 = 25$ and $35\ \mathrm{cm\,s^{-1}}$ agree well, which indicates that the nitridation kinetics was not intruded by external heat and/or mass-transfer effects.

A typical conversion curve obtained in fluidized-bed nitridation (Fig. 4) exhibits an induction period, followed by a rapid rise in the overall conversion. In most of the experiments, another increase in the reaction rate could be observed at conversions in the range 20%–30%. The reaction rate then gradually slows down, with the extent of the reaction not reaching

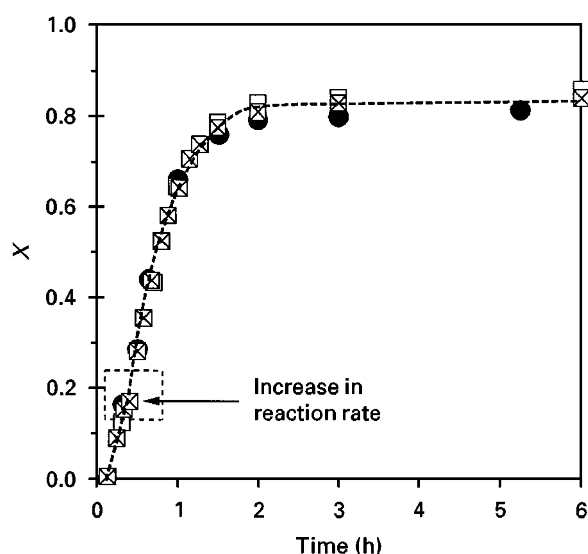

Figure 4 Reproducibility of results and effect of fluidizing velocity on nitridation at $1275\,^{\circ}\mathrm{C}$ in a N_2–10% H_2 gas mixture. The fluidizing velocities were (■, □) $u_0 = 25\ \mathrm{cm\,s^{-1}}$, and (●) $u_0 = 35\ \mathrm{cm\,s^{-1}}$.

100% even after an extended reaction time [22]. As it will be discussed in the subsequent sections, the conversion in the final nitridation stage in some cases asymptotically levels off, while in others it very slowly but continuously increases. For practical reasons, however, the overall conversion after which the conversion rate becomes only a few per cent per hour is defined in this work as the *final overall* or the *asymptotic conversion.*

The trend shown in Fig. 4 is in agreement with previously reported TGA results [31–33]. The existence of an induction period has usually been attributed to the native SiO_2 layer covering the silicon surface and hindering the nitridation [14, 18–20]. Sheldon *et al.* [33] have reported that a relatively small amount of oxygen leads to longer induction times. At the same time, however, these authors observed an induction period in the nitridation of unoxidized silicon samples as well. A closer look at literature data shows that the induction period becomes more pronounced as reaction temperature decreases.

The reactant pellets essentially maintained their original size and shape during nitridation [22, 35]. Because the ratio of the volume of Si_3N_4 formed per volume of silicon consumed is $Z = 1.216$ [37], the porosity of the pellet decreases with the progress of the reaction. For this reason, Ku *et al.* [38] and Pigeon and Varma [37] have stressed that the intra-pellet diffusion limitation may become an important rate-controlling factor in nitridation of compacted silicon grains by slowing the overall reaction rate [39].

Fig. 5 presents a BSE photo of a pellet sampled during the final stage of one of the runs under the conditions when the reaction practically seized off. The figure shows that the individual grains of the produced Si_3N_4 are much smaller than the original silicon grains (Fig. 1). In addition, the unreacted silicon is remarkably concentrated in the larger grains, regardless of their distance from the surface of the

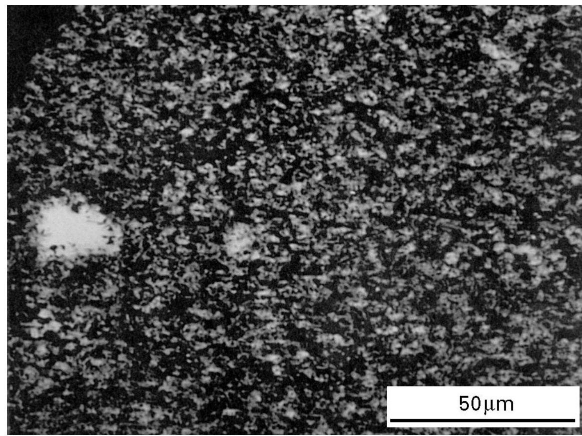

Figure 5 BSE image of cross-section of a reacted pellet sampled under conditions when nitridation practically seized off (white, silicon; grey, Si_3N_4; black, voids) [35]. The sample was nitrided for 6 h in 10% H_2–N_2 at 1250 °C to $X \approx 82\%$. A sample taken after 3 h showed $X \approx 79\%$.

pellet. This observation indicates that the reaction proceeded uniformly throughout the pellet rather than from the outer surface of the pellet inwards, which precludes macroscopic intrusion of the process by intra-pellet heat and/or mass-transfer effects. The finding that the conversion curves were unaffected by a pellet size [22] also supports this conclusion.

4.1. Effect of reaction temperature

Fig. 6 shows the effect of reaction temperature on the overall conversion of silicon, X, and on the yield of β-Si_3N_4 which is represented by mass fraction of this phase on the silicon free basis, W'_β. The data presented in this figure, all obtained using a N_2–10% H_2 gas mixture, indicate the following observations related to an increase in reaction temperature: (a) induction period decreases, with reaction starting almost immediately at 1300 °C; (b) the final overall conversion increases, and (c) the yield of the β-form decreases. Compared with the nitridation at 1200 °C, which terminates after approximately 5 h, the final nitridation stage at 1300 °C deviates slightly from the asymptotic behaviour (Fig. 6a).

It should be mentioned that at temperatures above 1300 °C, the α/β ratio in the product continues to increase, but the final overall conversion does not. For example, the XRD analysis of a sample nitrided for 2 h at 1350 °C (10% H_2–N_2, $u_0 = 35\ cm\,s^{-1}$) revealed $\approx 96\%$ of the α-form in the product, but the overall conversion of only $\approx 80\%$. If, however, the reaction is carried out up to $X \sim 30\%$ at a temperature in the range 1200–1300 °C, and then continued at higher temperatures (up to 1390 °C), almost complete conversion of silicon can be achieved in as short as 2.5 h [22, 35]. Therefore, a decrease in the asymptotic conversion observed at higher temperatures does not appear to be an intrinsic nitridation effect. It is possible that it is related to an increased contamination level of the bare silicon surface by the reactor parts made of alumina, which has been shown to be a significant oxygen source at high temperatures [16].

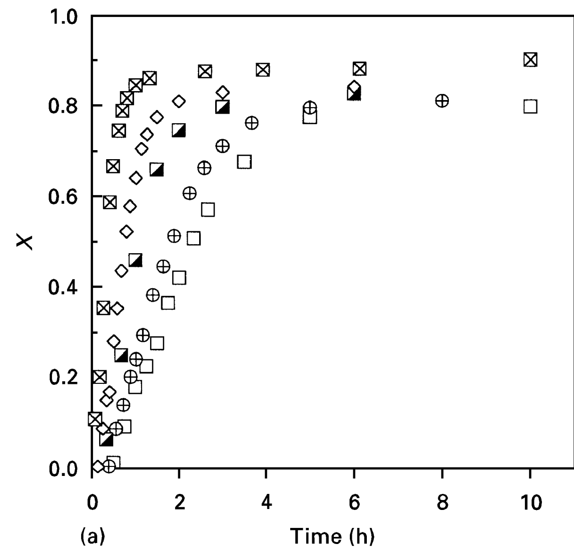

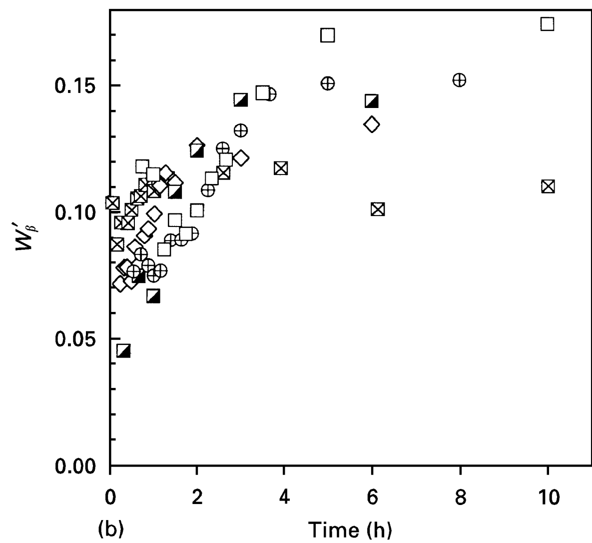

Figure 6 Effect of reaction temperature on the overall conversion of silicon, X, and mass fraction of the β-form in produced Si_3N_4 W'_β, (10% H_2–N_2; $u_0 = 35\ cm\,s^{-1}$ at 1300 °C, $25\ cm\,s^{-1}$ at all other temperatures). The temperatures studied were (□) 1200 °C, (⊕) 1225 °C, (◪) 1250 °C, (◇) 1275 °C, and (■) 1300 °C [35].

4.2. Effects of hydrogen and nitrogen

It has generally been accepted in the literature that the presence of hydrogen in a nitriding atmosphere enhances the nitridation reaction towards the formation of α-Si_3N_4 [15, 20, 40]. Jovanovic *et al.* [22] have reported that nitridation with a higher hydrogen concentration slows the reaction in the middle nitridation stage, increases the final overall conversion of silicon, and yields Si_3N_4 with a higher content of the α-form. It has been believed that the main role of hydrogen is in assisting the generation of gaseous SiO (an important reactant for the formation of α-Si_3N_4 [15, 40]) or in controlling the reaction exotherm by diluting nitrogen and acting as a heat acceptor [20].

The above-mentioned findings about the hydrogen effect were, however, all observed in the experiments with binary N_2–H_2 mixtures, where a change in concentation of one component (hydrogen) inevitably caused a change in concentration of the other (nitrogen). Hence, the results of such experiments could be

attributed to the role of hydrogen only in the case when neither the yield of the α-form nor the final extent of reaction are affected by the nitrogen concentration. In order to investigate separate effects of hydrogen and nitrogen concentrations on the overall conversion of silicon and on the α/β ratio in the product, two series of runs at 1250 °C were made: (a) the nitrogen concentration was fixed at 30% but the hydrogen concentration varied (5%, 10%, 30% and 50%), and (b) the hydrogen concentration was fixed at 10% but the nitrogen concentration varied (30%, 50%, 70% and 90%). In all of these experiments, argon was used as an inert balance as needed. The results of these runs are presented in Figs 7 and 8, respectively.

An interesting finding about the effect of hydrogen is presented in Fig. 7a: neither the induction period nor the initial reaction stage change with an increase in the hydrogen concentration. At the overall conversions greater than ~ 20%, however, the nitridation rate decreases as the hydrogen concentration increases. At the same time, the final overall conversions are approximately the same, regardless of a hydrogen content in the gas. In addition, as shown in Fig. 7b, the content of the β-form in the produced Si_3N_4 decreases only slightly (~ 3%) as the hydrogen concentration increases (it is difficult to estimate how significant the differences in Fig. 7b are because of the resolution of the quantitative XRD analysis [35]).

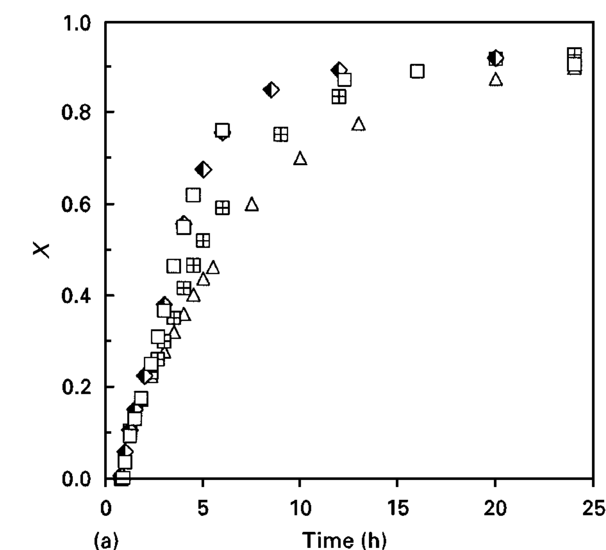

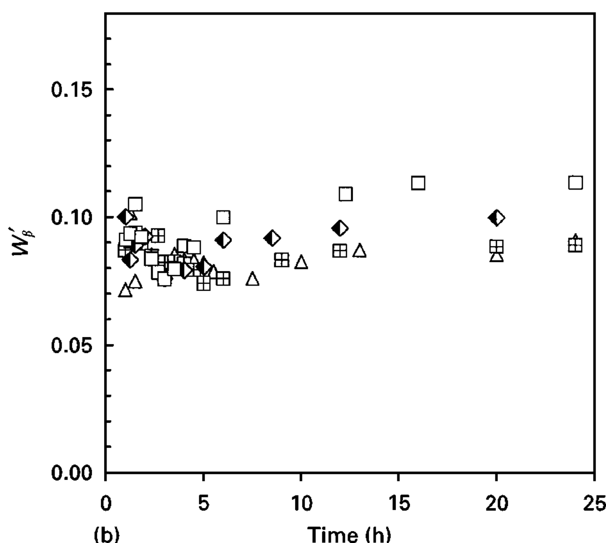

Figure 7 Effect of the hydrogen concentration in nitriding atmosphere on the overall conversion of silicon, X, and mass fraction of the β-form in produced Si_3N_4 W'_β, (1250 °C, 30% N_2–H_2–Ar). The hydrogen concentrations used were (□) 5%, (◆) 10%, (■) 30% and (△) 50% [35].

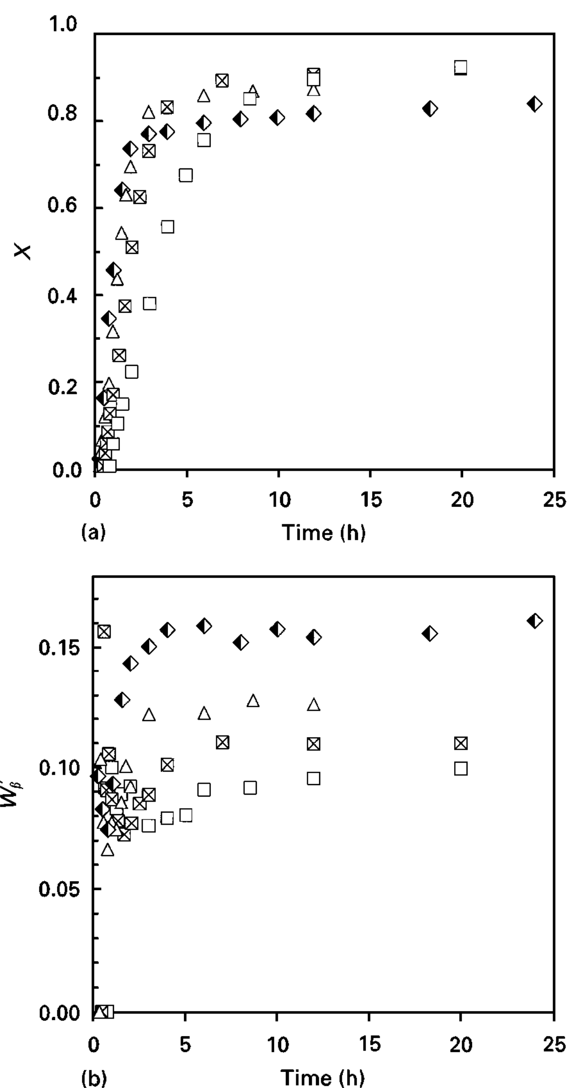

Figure 8 Effect of the nitrogen concentration in nitriding atmosphere on the overall conversion of silicon, X, and mass fraction of the β-form in produced Si_3N_4 W'_β, (1250 °C, 10% H_2–N_2–Ar). The nitrogen concentrations used were (□) 30%, (■) 50%, (△) 70% and (◆) 90% [35].

It should be noted that an attempt at nitridation of regularly pretreated silicon pellets but with no hydrogen present in the gas phase resulted in an extremely low nitridation rate at 1250 °C. This was demonstrated by the fact that the exothermic effect of the reaction, otherwise quite drastic, could not have been observed even after several hours. It is suspected that in the absence of hydrogen the oxygen from a nitriding atmosphere and/or the alumina reactor parts was sufficient to re-oxidize and passivate the silicon surface.

The findings about the hydrogen effect (Fig. 7) indicate that some of the previous investigators might have overlooked the effect of nitrogen concentration on the progress of nitridation. This possibility is further supported by Fig. 8, which shows the effects of

nitrogen concentration (at a constant concentration of hydrogen) on both the overall conversion of silicon and yield of the β-form in the product. It can be seen that as the nitrogen concentration increases, the nitridation rates in the initial and middle reaction stages also increase, but the final overall conversion decreases (Fig. 8a). Moreover, it is remarkable that the decrease in nitrogen concentration affects the final nitridation stage in the same way as does an increase in the reaction temperature (nitridation with 90% N_2 practically terminates after ≈ 3 h of the reaction, while the conversion curve of the experiment performed with 30% N_2 deviates from such an asymptotic trend). This observation is consistent with the results of Atkinson *et al.* [24] and of Myhre and Motzfeld [32] who investigated the effect of reaction pressure on the nitridation in pure nitrogen. The fact is, however, that it cannot be explained from a standpoint of chemical equilibrium [41]. At the same time, the results shown in Fig. 8b indicate that a more pronounced effect on the decrease in yield of the β-form is related to a decrease in nitrogen concentration as compared to an increase in hydrogen concentration (Fig. 7b). All these findings imply that exceeding the flammability level of hydrogen in a nitriding atmosphere ($\approx 5\%$ in nitrogen) has no advantage for either the kinetics of the process or the product distribution. This conclusion is important when considering the safety-related costs of a commercial process.

Another interesting observation provided by the data presented in Fig. 8a is a decrease in the induction period with an increase in the nitrogen concentration (a more detailed illustration is available elsewhere [35]). One of the explanations for this effect could be that nitrogen helps in disrupting the residual protective SiO_2 layer on the silicon surface (not completely removed during the pretreatment) by the reaction towards Si_2N_2O. From another viewpoint, it is possible that an increase in the nitrogen concentration enhances the nucleation of Si_3N_4, thereby facilitating initiation of the reaction. Further study is needed to clarify this finding, which eventually may lead to an explanation of a nature of the induction period.

5. Mechanism

5.1. Micro-structure of reacting pellet

Transmission electron micrographs of samples collected during one of the runs are shown in Figs 9 and 10. The conversion curve for that particular run is not presented in this work but it can be found elsewhere [22, 35].

As shown in Fig. 9a and b, in the early stage of reaction Si_3N_4 is being generated in the form of fine whiskers bridging silicon grains, as well as a layer developing on the silicon surface. The whisker-like product morphology, typical for chemical vapour transport processes, may imply that a gas-phase reaction between nitrogen and either silicon-vapour or SiO (in the presence of hydrogen) occurs during this nitridation stage [42]. The product layer on the silicon surface was found to be about 60 nm thick, although

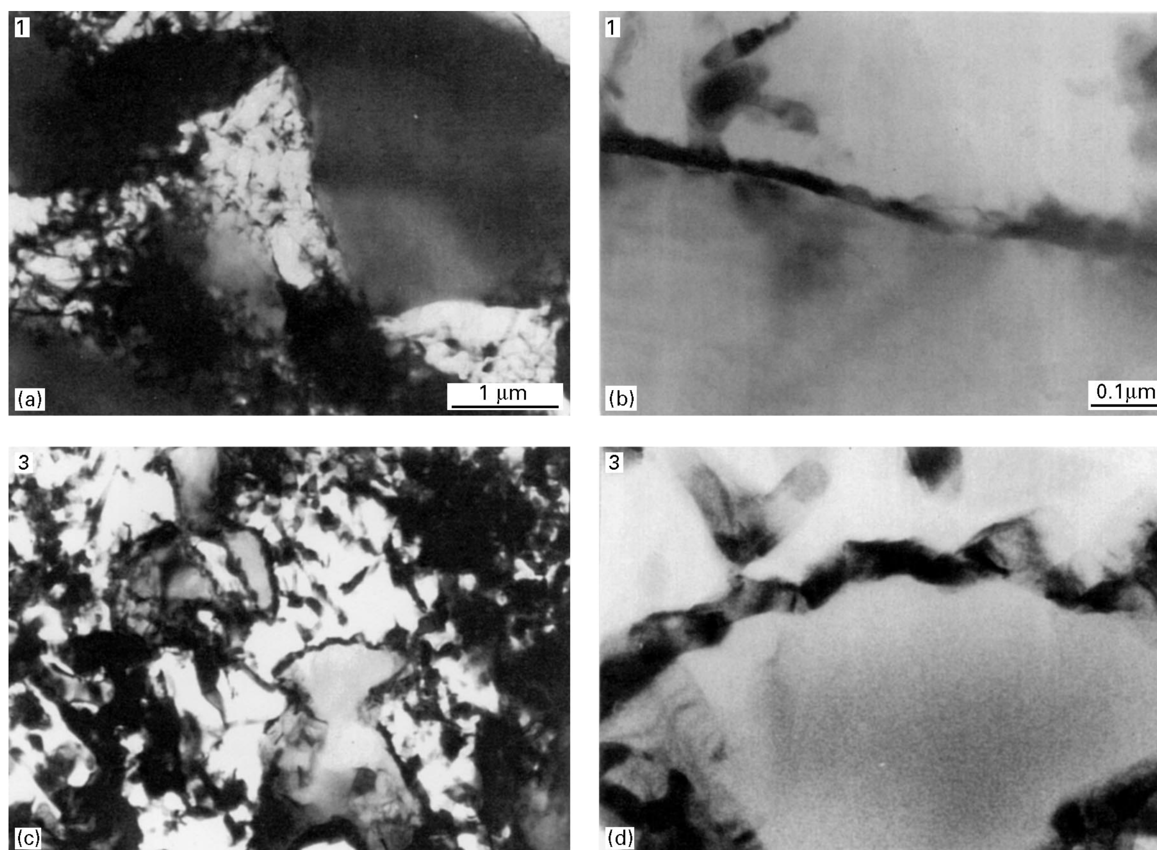

Figure 9 Transmission electron micrographs of samples converted to (a, b) $X \approx 11\%$ and (c, d) $X \approx 54\%$ in N_2–40% H_2 at 1300 °C ($u_0 = 25$ cm s^{-1}) [35]. Dark contrast designates Si_3N_4. (The magnifications of (c) and (d) are shown in (a) and (b), respectively.)

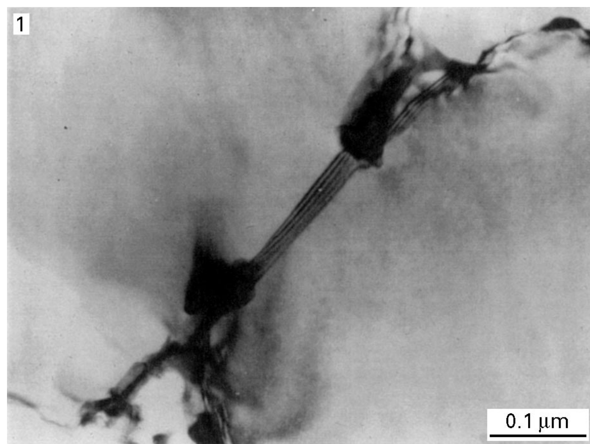

Figure 10 Growth of Si_3N_4 along grain boundaries within a polycrystalline silicon grain in a sample converted to $X \approx 11\%$ in N_2–40% H_2 at 1300 °C ($u_0 = 25$ cm s^{-1}) [35].

a thinner layer (≈ 20 nm) was also observed at a different location [30].

In this initial reaction stage, the product is also observed to grow along the grain boundaries between sintered silicon grains (Fig. 10). Because the product growth is associated with an increase in volume, it is possible that the reaction in these boundaries could disintegrate some of the silicon grains, thereby exposing a fresh silicon surface to nitrogen. This may be one of the explanations for the increase in the nitridation rate observed at $X \sim 20\%$–30% (Fig. 4).

The photomicrographs of the sample converted to $\approx 54\%$ (Fig. 9c and d) show that, even at this intermediate conversion, the silicon surface becomes almost completely and rather uniformly covered with a ≈ 60 nm thick Si_3N_4 layer, found to have a polycrystalline structure [30]. The silicon grains decrease in size, but only a part of the produced Si_3N_4 remains as the polycrystalline scale around the unreacted silicon. The rest of the product can be seen in the form of needle-like crystals filling the inter-grain space, that are, markedly, all of elongated shape and of similar thickness. The photomicrographs of a sample converted to $\approx 86\%$ (shown elsewhere [30, 35]) indicated the product mainly in the inter-grain voids. In this reaction stage, the thickness of the product layers on the silicon surface was found to be non-uniform, ranging up to ≈ 100 nm [30].

Koike and Kimura [30] have found that the product shown in Fig. 9 consists of α-Si_3N_4, regardless of its morphology (needles in inter-grain voids, surface layers on silicon grains). On the other hand, TEM electron beam diffraction analyses have shown that the nitride phase which tends to grow along grain boundaries in silicon is predominantly β-form [43]. The latter appears to be consistent with reported observations that have related a high α/β ratio with a high surface area of raw Si material [42]. Moreover, due to the absence of secondary phases at the Si/Si_3N_4 interface, Koike and Kimura [30] have also suggested that the α-form is directly produced via a silicon–nitrogen reaction, without forming any intermediate phase.

It is important to point out that the presence of the needle-like product in the inter-grain voids (Fig. 9c and d) should not be attributed to the crackling of the product scale due to a sudden temperature change during the sampling. This possibility is precluded by essentially the same BET areas of the samples converted in one of the runs to a same level, but one of them taken at reaction temperature (4.50 m^2 g^{-1}), while the other was obtained after the bed had been slowly cooled to room temperature (4.43 m^2 g^{-1}). On the other hand, the similar shape and thickness of the product needles in the inter-grain space, in conjunction with the fact that the observed thickness of the product layers does not correspond to the overall conversion [30], may indicate that nitridation occurs through subsequent spallings of the product scale from the silicon surface [30]. This hypothesis is also supported by direct physical evidence presented elsewhere [30, 35].

According to Thompson and Pratt [27], the spalling of the produced Si_3N_4 from the silicon grains can be explained by the increase in volume on forming the nitride. Based on the elastic misfit strain between the silicon and Si_3N_4 lattices, Koike and Kimura [30] have predicted that any pre-existing crack at the Si/Si_3N_4 interface would propagate with an increase in nitride thickness. According to the calculations of these authors, the nitride detaches from the silicon surface when it reaches the thickness of 57 nm. This estimate for the critical nitride thickness is in reasonable agreement with the experimental evidence (20–100 nm) [30], as well as with the observations by previous investigators [27, 29]. Moreover, Thompson and Pratt [27] have suggested that the spalling of the product scale is a key factor for the reaction to proceed, because the process kinetics is controlled by the nitrogen diffusion towards the silicon where the product grows.

5.2. Rate-controlling step

Fig. 9 (the physical evidence of the mechanism of nitridation) and Fig. 8a (the effect of nitrogen concentration on the overall conversion) preclude the possibility that the silicon transport through the product layer controls the overall nitridation rate. If the supply of silicon (vapour, atoms or ions) to the reaction site presents the rate-controlling step, then the reaction rate should become independent of nitrogen concentration as soon as the product scale develops over the silicon surface. The data shown in Fig. 8a indicate, however, that at intermediate conversions ($\sim 50\%$), when silicon already becomes rather uniformly covered with the product (Fig. 9c and d), the conversion curves become steeper, i.e. the nitridation rate increases as the nitrogen concentration increases. Assuming that the effective surface areas of silicon are about the same at the same conversions in all of the experiments shown in Fig. 8, it means that the transport of silicon to the gas/Si_3N_4 interface cannot be the rate-controlling step. At the same time, the data in Fig. 8a imply that this step could be any of the following: (i) surface reaction(s) at the outer nitride

surface producing active nitrogen species, (ii) the transport of such species through the Si_3N_4 scale towards the Si/Si_3N_4 interface, or (iii) a reaction at the Si/Si_3N_4 interface.

Owing to a likely higher diffusion mobility of hydrogen species, the presence of hydrogen in the reacting system may decrease the diffusion rate of nitrogen species through the polycrystalline product scale and along the grain boundaries in the polycrystalline silicon grains. The latter could be reflected by a delayed disintegration of the silicon grains due to a slower product growth along these boundaries. At the same time, a higher hydrogen concentration may also hinder the chemisorption of nitrogen at the external nitride surface. Therefore, the observed hydrogen effect on the second nitridation stage (Fig. 7a) could qualitatively explain any of the rate-controlling steps postulated above. In addition, it is possible that all of these mechanisms participate in determining the overall reaction rate because of the observation that nitridation proceeds through subsequent spallings of the product scale from the silicon surface.

At present, however, neither the form of the active nitrogen species nor the exact transport mechanism of such species towards the Si/Si_3N_4 interface could be specified. Detailed research addressing these questions has been reported for the case of thermal growth of thin Si_3N_4 films, but utilizing NH_3 as a nitrogen source instead of N_2–H_2 mixtures [44]. The fact is that the reported self-diffusion coefficients of nitrogen through either single α- or β-Si_3N_4 crystals [45] are so small that they cannot explain the observed nitridation rates [35].

The existence of grain boundaries in the polycrystalline nitride scale, however, could increase the overall diffusion coefficient of nitrogen by several orders of magnitude [45, 46]. Faults and impurities in the product layer may cause a similar effect by decreasing the activation energy of the diffusion process [47]. In addition, nitridation takes place in the presence of silicon, which has a considerable number of intrinsic charge carriers at reaction temperatures ($\approx 10^{19}$ cm^{-3} at 1200–1400 °C [48]). This, in conjunction with the fact that the bonds in Si_3N_4 are partly ionic [49], indicates that a possible role of charged nitrogen species in the nitridation should not be neglected. In general, the transport of such species could be significantly facilitated by various electrostatic effects [50, 51] that may also affect an apparent activation energy of the overall process [52]. In this light, trace impurities in raw silicon material might have an additional role in the nitridation by serving as dopants that control generation of additional charge carriers in the silicon.

5.3. Asymptotic conversion

Understanding the conditions leading to the asymptotic behaviour of the overall conversion is pertinent to designing an efficient practical application, as well as to elucidating the mechanism of the nitridation process. In the literature, the diminishing reaction rate in the final nitridation stage has usually been attributed to the complete coverage of the silicon surface by the product scale [24, 27, 32]. This explanation, however, does not seem to be applicable to the results of this study, because of the observation that the reaction is still considerably fast even when almost the entire silicon surface becomes covered by the nitride (Figs 6–8 and 9b). Although the role of reaction conditions in the variability of the final extent of the reaction is not clear, some of the factors that may reduce the overall nitridation rate are discussed below.

The amount of silicon captured in very large grains lowers the overall reaction rate because of the small specific surface area of such grains. The finding that the majority of the unreacted silicon is observed in the largest silicon grains (Fig. 5) suggests that the grain-size distribution in a reacting pellet may be a key parameter determining the final overall conversion. In any case, the variability in the asymptotic conversion with reaction temperature and bulk nitrogen concentration (Figs 6 and 8) implies that the fraction of larger grains in the pellets and/or the overall contribution of the grains to the reaction due to non-intrinsic structural factors vary with experimental conditions.

It is suspected that the voids sealed between the product scale and the silicon surface may interrupt the nitrogen transport to the silicon surface, and hence decrease the overall nitridation rate [52]. Atkinson *et al.* [24] have attributed the formation of such voids to the product growth over the depressions in the silicon surface, formed by surface removal of silicon around growing product nuclei. The voids could also be sealed by the subsequent sintering of the detached product crystallites around the silicon grains after prolonged reaction times [52]. The viability of the latter scenario increases as the size of the product crystallites decreases. In this light, higher reaction temperatures and/or lower nitrogen concentrations could increase the asymptotic conversion by promoting coarser product crystallites, as observed by Atkinson *et al.* [24]. It should be noted that the formation of the voids appears to be more pronounced as the size of silicon grains increases [42]. The results of this work also indicate that the voids can be observed around the largest grain in the cross-section shown in Fig. 5, while they could not be seen in and around intermediate-sized grains in Fig. 9b.

Koike and Kimura [30] have stressed the possibility that spalling of the product scale may not occur as the silicon grains decrease in size with the progress of nitridation. This would decrease the rate of nitridation of the silicon grains when they become small enough, if the rate is controlled by the diffusion of nitrogen through the product scale. On the other hand, the surface migration of the silicon atoms [24], possible crackling of the silicon grains during reaction, and the presence of impurities in both the nitriding atmosphere and silicon could create such portions of the silicon surface that are not thermodynamically favoured for the nucleation of the product. In this case, a part of the silicon surface would contribute less to the reaction, even when it is fully exposed to nitrogen.

5.4. The α/β question

The data presented in Figs 6 and 8 suggest that the increase in the α/β ratio might be related to the increase in the final overall conversion. This, combined with the finding that the β-form tends to grow along grain boundaries between sintered silicon grains, and the fact that the presence of coarse silicon grains lowers the final extent of reaction, suggests the possibility that disintegration of silicon grains during the reaction may be one of the factors controlling the α/β ratio. In this light, an increase in the α/β ratio with an increase in reaction temperature could be attributed to a faster product growth along the grain boundaries in the polycrystalline silicon grains, and with it associated thermal stress facilitating disintegration of such grains. This work, however, does not offer any conclusive explanation which would distinguish between the α/β formation mechanisms, or clarify the role of nitrogen dilution in increasing the α/β-ratio.

6. Modelling

6.1. Previous work

Ambiguity regarding the mechanism of the nitridation reaction could be the reason for a number of different kinetic approaches taken, and a variety of models proposed to describe the conversion of silicon into Si_3N_4. Typically, nitridation has been approached as a multi-step process. The initial reaction stage has usually been described by an approximately constant rate law, while the subsequent stage has been considered as the nucleation and growth [53], simultaneous diffusion and sintering [54], or the chain nucleation and "branching" of the nitride scale [32]. Some studies [24, 32] have shown that in this nitridation stage the conversion of silicon could be reasonably well fitted by the assymptotic exponential law [55]. Although most of the reported models have been based on the kinetics of the overall conversion of silicon, Rosetti and Denkewicz [56] have proposed different models for the formation of the α- and β-forms. Remarkably, despite the early microstructural evidence about the nitride layer developing on the surface of the silicon grains [24, 27], none of the reported studies have confirmed the applicability of the Shrinking Core Model with product layer diffusion control [57]. A recent attempt [37] at using essentially the same Sharp Interface Model [58, 59] has been proved inconsistent with experimental observations [60].

6.2. Preliminary considerations

The discussion from previous sections has shown that the available information about the mechanism of direct nitridation of silicon is insufficient for elaborate quantitative modelling of this process. A particular problem arises in the attempts at distinguishing intrinsic process kinetics from structural factors occurring during the nitridation, and deciding which of these dominates the overall effect on the process rate. This difficulty was especially encountered in this work because of uncertain information about the size distribution of the silicon grains in the precursor pellets. Moreover, it is likely that product growth could disintegrate some of these grains, thereby causing a dynamic change in the effective reaction surface area by generating new grains. Because the final overall conversion apparently depends on a fraction of larger grains in the precursor pellet (Fig. 5), the variability in the final overall conversion with reaction conditions could not be explained with certainty.

Although the fraction of larger grains in a multimodal size distribution may strongly affect the final overall conversion, at the same time it may not significantly affect either the total surface area of the grains or the mean grain size. This is demonstrated by the results shown in Fig. 2, where the two substantially different size distributions A and B have essentially the same specific surface areas and the means. Therefore, relating nitridation rate to the kinetic expressions that are based on the mean grain size [35] appears to be inappropriate for this case.

Another problem in analysing the data from this study is the unknown nature of the transition in the kinetic behaviour, commonly observed in the conversion range $X \sim 20\%$–30% (Figs 4, 6a, 7a and 8a). It is not clear whether this transition reflects a change in nitridation mechanism, or if it should be attributed to the effects of non-intrinsic structural factors. The initial reaction stage appears to be distinct from the rest of the data points (Fig. 4), with the reaction rate increasing with an increase in temperature and/or nitrogen concentration (Figs 6a and 8a). At the same time, an increase in hydrogen concentration seems only to extend the duration of this reaction stage, without affecting the rate (Fig. 7a). Because of an insufficient resolution of the experimental data points at the onset of reaction, this nitridation stage could not be further investigated.

On the other hand, preliminary testing of various kinetic models on the rest of the conversion curves has shown that the overall conversion in the second nitridation stage can be well described by the asymptotic exponential law as

$$X = X_f(1 - e^{-\kappa \bar{t}}) \quad (2)$$

In Equation 2, X_f designates the asymptotic final conversion, κ is a constant, and $\bar{t} = t - t_0$ represents the actual reaction time, t, corrected by the additional parameter, t_0, which is introduced in order to account for the induction period and the initial nitridation stage. The typical fits according to Equation 2 [61] are compared with the corresponding conversion curves in Fig. 11, which demonstrates reasonable agreement between the fit and the experiment. The discrepancy could be seen only for extended reaction times due to a slight deviation of the experimental data from the asymptotic behaviour (particularly for the data obtained at lower nitrogen concentrations and/or higher temperatures).

The conversion law given by Equation 2 has been proposed in the literature for describing gas–solid reactions controlled by the nucleation and branching of the product scale [32], or by simultaneous gas diffusion through pores and pore closure [55]. Although the latter could account for a decrease in the

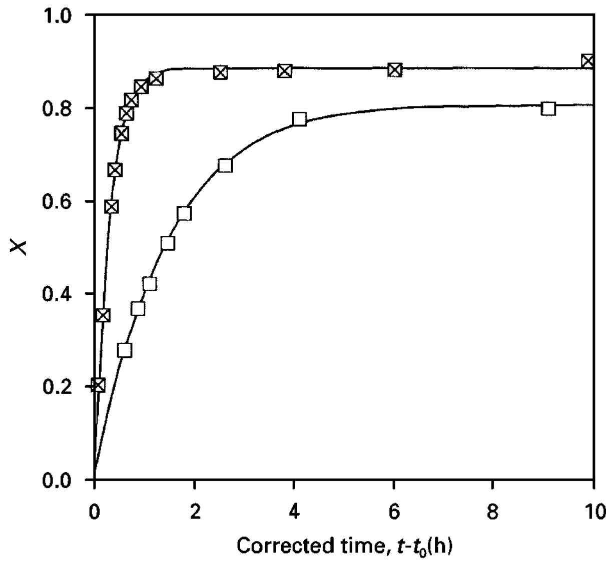

Figure 11 Comparison between experimental data (symbols) and (——) prediction by Equation 2 at the temperature (□) 1200 °C and (■) 1300 °C (N_2–10% H_2) [35].

nitridation rate due to possible sintering of the product needles around the silicon grains, yet another approach has been developed in an attempt to describe the presented kinetic results more specifically. A substantial amount of evidence presented in the previous sections has indicated that the transport of nitrogen from the gas phase to the Si/Si_3N_4 interface and/or the reaction at this interface control the overall nitridation rate, and that nitridation proceeds through subsequent spallings of the nitride scale from the silicon surface. Therefore, these were the starting assumptions in the analysis that follows. Also, nitridation is approached as the overall process producing both Si_3N_4 phases because this work has not provided the basis for distinguishing between the α/β formation mechanisms.

6.3. Overall nitridation rate and reaction surface area

Let the size distribution of silicon grains in a reacting porous pellet be given as a two-dimensional array of length M, containing mass fractions of grains, w_m, that have corresponding equivalent mean initial radii, $R_{m,0}$. Furthermore, assume that the nitride scale grows uniformly over the surface of these grains up to the thickness δ_{max}, after which it detaches from the grains so a fresh silicon surface is exposed. The radius, r_m, of the unreacted core of the grains that originate from a size range m can be then related to the outer grain radius, R_m, and instantaneous nitride scale thickness, δ_m, by the following relationships

$$r_m = R_{m,0}(1 - X_m)^{1/3} = R_m(1 - x_m)^{1/3}$$

$$R_m = R_{m,0} - \delta_{max}\left[\mathrm{int}\left(\frac{R_{m,0} - r_m}{\delta_{max}}\right)\right]$$

$$\delta_m = R_m - r_m \leqslant \delta_{max} \tag{3}$$

In the above equations, X_m represents the overall conversion of the size range m, while x_m designates the fractional conversion of that size range with respect to the outer grain diameter. Therefore, if two successive spallings of the product scale occur at moments t_{i-1} and t_i, a change in x_m within a time scale θ defined by

$$0 \leqslant \theta \leqslant t_i - t_{i-1} \tag{4}$$

can be expressed as [62]

$$x_m = \frac{k_{ex}}{R_m}\theta \tag{5}$$

for surface reaction at the gas/Si_3N_4 interface controlling,

$$1 - 3(1 - x_m)^{2/3} + 2(1 - x_m) = \frac{k_{diff}}{R_m^2}\theta \tag{6}$$

for diffusion through the product scale controlling, and

$$1 - (1 - x_m)^{1/3} = \frac{k_r}{R_m}\theta \tag{7}$$

for reaction at the Si/Si_3N_4 interface controlling. It should be noted that the above equations do not account for the difference between the volumes of the nitride formed and silicon consumed by the reaction, because it can be shown that ignoring this difference has essentially no impact on the trend of the conversion curves [60]. For a particular nitrogen concentration, k_{ex}, k_{diff}, and k_r are constants described in detail elsewhere [62]. Once these constants are known, the above equations enable calculation of the overall conversion of silicon for a particular mechanism at any time as

$$X = \sum_{m=1}^{M} w_m X_m \tag{8}$$

In order to develop an integral expression $X = X(t)$ for the overall conversion, it is convenient to define the overall nitridation rate (r''_{Si}) with respect to the initial amount of silicon, $N_{Si,0}$, as

$$r''_{Si} = \frac{N_{Si,0}}{S}\frac{dX}{dt} \tag{9}$$

and a mean decrease in the radii of the grains, δ_r, as

$$\delta_r = \frac{\sum_{m=1}^{M}(R_{m,0} - r_m)S_m}{\sum_{m=1}^{M} S_m} = \frac{1}{S}\sum_{m=1}^{M}(R_{m,0} - r_m)S_m \tag{10}$$

In Equation 10, S_m represents the contribution of a size range m to the total surface area, S, defined depending on a reaction mechanism to be considered. For reaction at the unreacted core controlling, S_m should represent the area of the Si/Si_3N_4 interface, $S_{Si,m}$, while for reaction at the external nitride surface controlling it needs to be calculated as the surface of the gas/Si_3N_4 interface, $S_{SN,m}$. Because there is no unique definition for S_m in the case of diffusion through the product layer controlling, this mechanism

is chosen to be considered based on $S_m \equiv S_{\mathrm{Si},m}$. The total areas of the Si/Si_3N_4 and the gas/Si_3N_4 interfaces (S_{Si} and S_{SN}, respectively) are related to the initial surface area of the grains, S_0, as [35]

$$\frac{S}{S_0} = \frac{\sum_{m=1}^{M} \frac{w_m}{R_{m,0}} \chi_m}{\sum_{m=1}^{M} \frac{w_m}{R_{m,0}}}$$

$$\chi_m = \begin{cases} (1 - X_m)^{2/3} \rightleftharpoons S \equiv S_{\mathrm{Si}} & \text{(11a)} \\ \left(\dfrac{R_m}{R_{m,0}}\right)^2 \rightleftharpoons S \equiv S_{\mathrm{SN}} & \text{(11b)} \end{cases}$$

Among the kinetic laws discussed in this section, that for the mechanism controlled by a reaction at the core is the only unaffected by the spalling of the product scale. It can be shown that the constant reaction rate in this case relates to the product growth rate as [62]

$$\frac{d\delta_r}{dt} = k_r = \frac{r''_{\mathrm{Si}}}{\rho_{\mathrm{Si}}} \quad (12)$$

which enables rewriting Equation 9 as

$$\frac{dX}{dt} = \frac{\rho_{\mathrm{Si}}}{N_{\mathrm{Si},0}} S \frac{d\delta_r}{dt} = \frac{S}{V_0} k_r \quad (13)$$

with ρ_{Si} and V_0 designating the molar density of silicon and the initial volume of the silicon grains, respectively. Therefore, in order to develop an integral expression $X = X(t)$ for this case, it is sufficient to know a relationship $S = S(X)$.

6.4. Computer simulation and fitting of the conversion curves

The algorithm presented in the previous section has been implemented into a FORTRAN program in order to explore the effects of δ_{max}, size distribution, and a reaction mechanism on the overall conversion of silicon. Because the relevant kinetic constants have been chosen arbitrarily, the computer-generated conversion curves could only be qualitatively compared on an arbitrary time scale.

Fig. 12 presents the results of simulating diffusion-controlled conversion of the two grain-size distributions A and B (shown in Fig. 2) for different values of δ_{max} that have been chosen based on the experimental observations. These results indicate the following:

(a) the trend of the calculated conversion curves (Fig. 12a) is similar to the trend of the experimental data (Fig. 4), with a noticeable increase in reaction rate seen at $X \sim 20\%$–30% in agreement with the experimental observations;

(b) the presence of coarser grains in the distribution B lowers the final overall conversion, and causes the pseudo-asymptotic conversion trend (Fig. 12a);

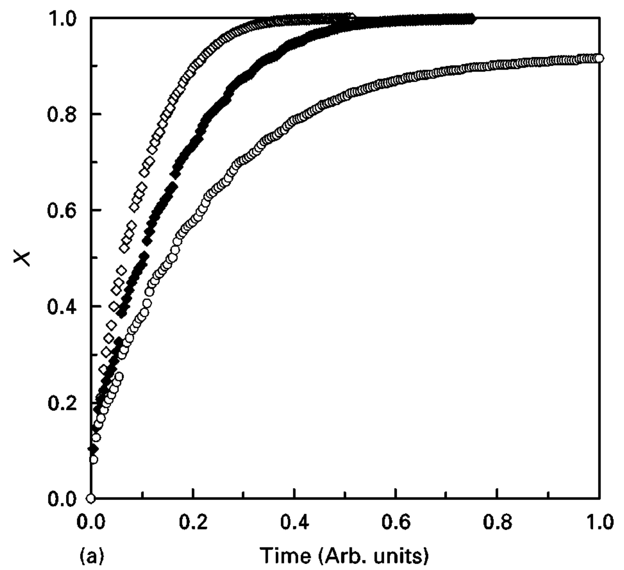

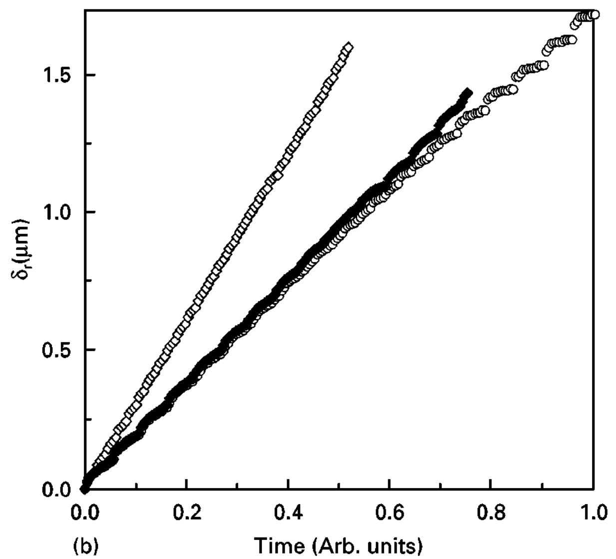

Figure 12 Relationships (a) $X = X(t)$ and (b) $\delta_r = \delta_r(t)$ simulated for diffusion-controlled conversion of the grain-size distributions shown in Fig. 2. The calculations are illustrated for (◇) distribution A and $\delta_{max} = 60$ nm, (◆) distribution A and $\delta_{max} = 100$ nm and (○) distribution B and $\delta_{max} = 100$ nm.

(c) an increase in δ_{max} has essentially no effect on the final overall conversion (Fig. 12a), but it affects the conversion curves in the same way as does an increase in hydrogen concentration (Fig. 7);

(d) for the investigated range of δ_{max}, the product growth rate could be considered constant (Fig. 12b), i.e. it can be approximated by Equation 12 derived for the mechanism controlled by a reaction at the core.

The last observation further implies that for the investigated range of δ_{max}, the diffusion controlled mechanism adjusted for the spalling of the product scale may be considered as the mechanism controlled by a first-order reaction at the core. For this case, it is convenient to introduce an apparent reaction-rate constant with respect to the unknown diffusing nitrogen species, N_x, as

$$k_{N_x} = \frac{D_{\mathrm{eff}}}{t} \int_0^t \left[\frac{1}{S} \sum_{m=1}^{M} \frac{1}{\delta_m} S_m \right] d\tau = \frac{D_{\mathrm{eff}}}{\hat{\delta}} \quad (14)$$

and to express the overall nitridation rate as

$$r''_{Si} = br''_{N_x} = b(k_{N_x}c_{N_x})\hat{\delta} \quad (15)$$

In Equations 14 and 15, $\hat{\delta}$ represents the equivalent thickness of the product scale over the surface of the unreacted silicon, D_{eff} designates the effective diffusion coefficient of the nitrogen species, N_x, through the product scale, b is the number of silicon moles reacting per mole of N_x, and c_{N_x} is the concentration of N_x at the external nitride surface. Because the diffusion coefficient D_{eff} may reflect the overall contribution of two parallel nitrogen transports that occur by lattice and by grain-boundary diffusion, it can be represented as

$$D_{eff} = \frac{1}{S}(D_l S_l + D_{gb} S_{gb}) = D_l \hat{S}_l + D_{gb} \hat{S}_{gb} = D_l + (D_{gb} - D_l)\hat{S}_{gb} \quad (16)$$

where D_l represents the lattice diffusion coefficient, D_{gb} is the grain-boundary diffusion coefficient, while $\hat{S}_l$ and $\hat{S}_{gb}$ designate the fractions of the total reaction surface areas occupied by lattices, S_l, and by grain boundaries, S_{gb}, respectively. It should be recognized that the ratio $\hat{S}_{gb} = S_{gb}/S$ can be directly related to the specific number of crystals in the polycrystalline product scale per surface area of silicon. This specific number, however, may be dependent on the relative magnitudes of the rates of nucleation and of lateral product growth [24]. Therefore, $\hat{S}_{gb}$ may be a function of both reaction temperature and nitrogen concentration, which implies that D_{eff} and k_{N_x} may be concentration dependent as well (Equations 16 and 14).

The above discussion has shown that Equation 13 can be utilized for the case of diffusion-controlled nitridation as well. Hence, the only remaining information required to integrate this equation is a relationship $S = S(X)$, reported to differ considerably for the reaction of grains having a size distribution as compared to the reaction of single size grains [63]. This relationship has also been explored, and typical results are illustrated in Fig. 13. The figure shows that S decreases faster at lower conversions, which should be attributed to the presence of sub-micrometre silicon grains in both size distributions. On the other hand, the presence of coarse grains in the distribution B decreases S to essentially zero already at $X \approx 92\%$. Markedly, both graphs in Fig. 13 indicate that for the conversions in the range $X > 20\%$ the relationship $S = S(X)$ could be considered linear, i.e. represented as

$$S \approx S_0^*(1 - f_{rs}X) \quad (17)$$

where S_0^* designates extrapolated initial reaction surface area, while f_{rs} reflects the rate of a decrease in S with X. One may show that integrating Equation 13 with the help of Equations 17 and 12 yields the result

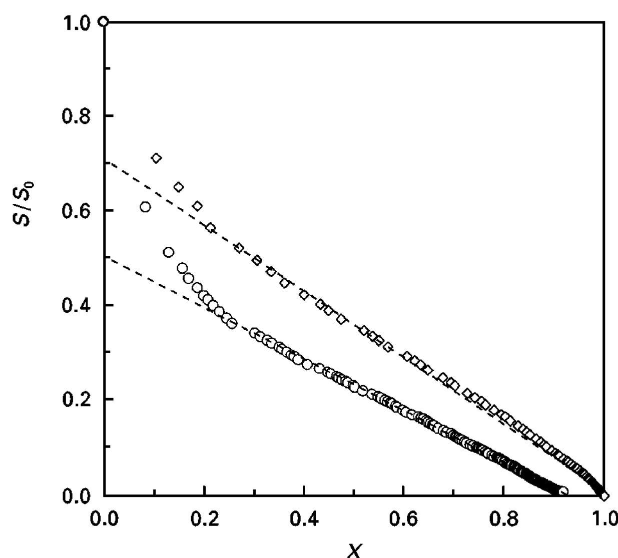

Figure 13 Relationships $S = S(X)$ simulated for diffusion-controlled conversion of the grain-size distributions shown in Fig. 2. The calculations are illustrated for (◇) distribution A and $\delta_{max} = 60$ nm, (○) distribution B and $\delta_{max} = 100$ nm.

equivalent to Equation 2, with

$$X_f = \frac{1}{f_{rs}}$$

$$\kappa = \left(f_{rs}\frac{S_0^*}{V_0}\right)_{const} \quad k_r = \left(f_{rs}\frac{S_0^*}{N_{Si,0}}\right)_{const} r''_{Si} \quad (18)$$

It can be shown that the analysis of the mechanisms controlled by reaction at the core and by reaction at the external nitride surface yields smoother conversion curves that are less similar to the experimental data. In particular, these two mechanisms do not reflect an increase in nitridation rate at conversions $X \sim 20\%$–30%, thus this increase could be explained only by crackling of the silicon grains during nitridation. However, it can be shown that the relationships $S = S(X)$ can be approximated by Equation 17 for these two cases as well. Recognizing that for both of these cases r''_{Si} is constant, that further implies that Equations 2 and 18 could fit all the mechanisms discussed in this work. The main reason for this is in the fact that δ_{max} is small relative to the size of the silicon grains. Therefore, none of the discussed nitridation mechanisms could be discriminated without additional evidence.

6.5. Dependence of nitridation rate on nitrogen concentration and temperature

The parameters f_{rs} and S_0^* have been introduced in the previous section as an intrinsic feature of a particular size distribution of the silicon grains that react according to a particular conversion mechanism. Assuming that Equations 2 and 18 may be applied to the actual nitridation as well, then the experimentally observed variability in X_f implies that these two parameters also depend on a set of reaction conditions. In other

words, f_{rs} and S_0^* reflect not only the intrinsic nitridation kinetics and the properties of the size distribution of the silicon grains, but also other factors that affect the overall nitridation rate (some of those are discussed in Section 5.3). In particular, these parameters may be affected by a possible crackling of the silicon grains during nitridation. Therefore, although f_{rs} can be conveniently eliminated by introducing the new parameter K^o as

$$K^o = K^o(c_{N_2}, c_{H_2}, T) = \kappa X_f = \frac{S_0^*}{N_{Si,0}} r''_{Si} \qquad (19)$$

the dependence of r''_{Si} on c_{N_2} and T could not be explored with certainty without estimating S_0^*. On the other hand, because of a rather narrow investigated range of the asymptotic conversions ($\sim 10\%$) it is reasonable to assume that S_0^* does not vary significantly with reaction conditions. In this case, the dependence of r''_{Si} on c_{N_2} and T could be approximated by the dependence of K^o on these parameters.

If S_0^* could be considered constant, the dependence of K^o on c_{N_2} illustrated in Fig. 14 indicates that r''_{Si} is proportional to c_{N_2}. This then may suggest that either chemisorption of nitrogen at the external nitride surface or a reaction of non-dissociated nitrogen at the Si/Si_3N_4 interface control the nitridation rate. At the same time, however, the proportionality between r''_{Si} and c_{N_x} could support diffusion-controlled nitridation kinetics as well. It should be recognized that in that case, the dependence $r''_{Si} = r''_{Si}(c_{N_2})$ could be the result of superimposed dependence of k_{N_x} and c_{N_x} on c_{N_2} (Equations 16, 14 and 15). Therefore, the linearity between r''_{Si} and c_{N_2} does not necessarily imply that non-dissociated nitrogen diffuses through the product scale. In addition, the form of nitrogen species that diffuses by lattice diffusion may differ from the form of nitrogen species that diffuses by grain-boundary diffusion. All these considerations, in conjunction with the uncertainty regarding S_0^*, place the discussion of an

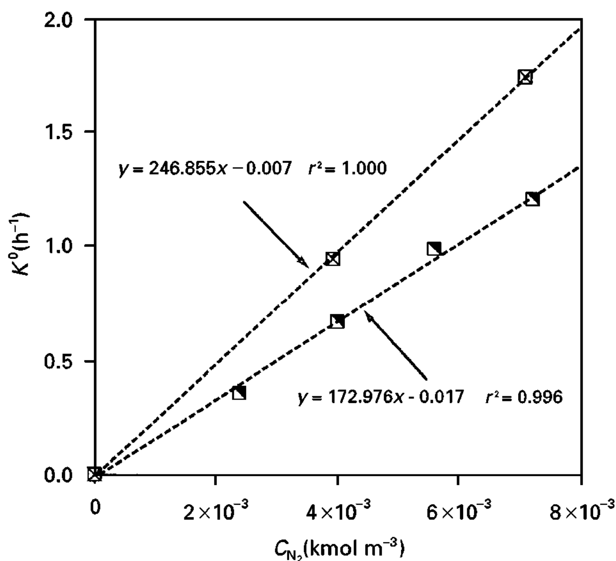

Figure 14 Dependence of K^0 on bulk nitrogen concentration in 10% H_2–N_2–Ar mixtures at (◪) 1250 °C and (■) 1275 °C [35].

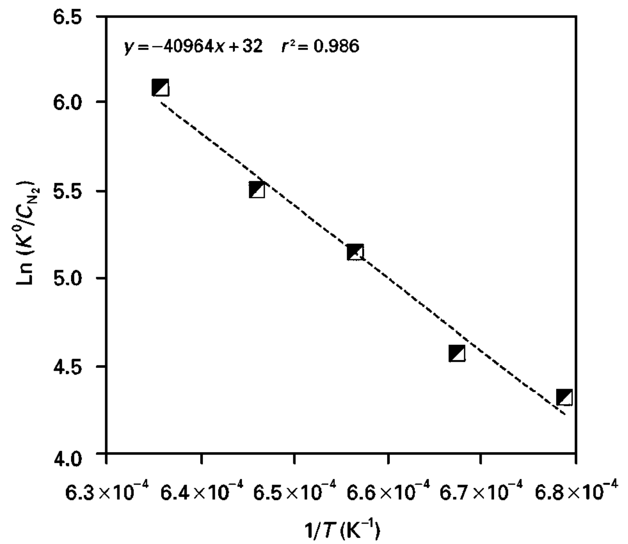

Figure 15 Evaluation of an apparent activation energy of nitridation in a 10% H_2–N_2 atmosphere [35].

intrinsic nitridation dependence on c_{N_2} beyond the scope of this work.

Based on the relationship between K^o (evaluated at constant c_{H_2}) and c_{N_2}, the temperature effect brought into K^o by c_{N_2} may be eliminated. Therefore, an apparent activation energy of the nitridation process, E_{app}, can be determined by plotting Ln (K^o/c_{N_2}) versus $1/T$ and assuming that the Arrhenius-type temperature dependence of r''_{Si} dominates temperature dependence of S_0^*. A reasonable linearity in Fig. 15 indicates that in the temperature range investigated (1200–1300 °C) the nitridation process could be considered as having the apparent activation energy of $E_{app} \approx 340\ \text{kJ mol}^{-1}$.

7. Conclusions

A fluidized-bed nitridation of pelletized silicon grains having a wide size distribution was carried out in the temperature range 1200–1300 °C. N_2 (30%–90%)–H_2 (5%–50%)–Ar (inert balance) mixtures were used as the nitriding gas at atmospheric pressure. The effects of reaction temperature and H_2–N_2 composition in the nitriding gas on the overall conversion of silicon and the yields of α- and β-Si_3N_4 were investigated. This study has shown that, provided a suitable silicon precursor, a fluidized-bed presents a convenient reactor for the production of Si_3N_4 with a high α/β ratio and with the amount of unreacted silicon controlled by the reaction temperature and composition of the nitriding atmosphere. The findings are summarized as follows.

1. The reaction is initiated after an induction period which becomes shorter with an increase in reaction temperature and/or an increase in nitrogen concentration, but remains unaffected by an increase in the hydrogen concentration. The reaction then proceeds in two consecutive stages, with a break point designated by an increase in reaction rate in the conversion range $\sim 20\%$–30%. It is not clear whether this transition in the kinetic behaviour reflects a change in nitridation mechanism, or if it should be attributed to the effects of non-intrinsic structural factors. The

kinetics of the initial stage was not investigated in this work; the second nitridation stage can be approximated reasonably well by the asymptotic exponential conversion law [55].

2. Nitridation proceeds uniformly throughout the individual porous silicon precursor pellets having sizes in the range investigated. The unreacted silicon is observed mainly in the largest grains in the pellets. The micro-structure of a sample collected during the early stage of the reaction indicates (i) the development of product layers over the silicon grains, (ii) product growth along the grain boundaries between sintered silicon grains, and (iii) whisker-like product in the inter-grain space. The latter suggests the possibility that, in this reaction stage, part of the product is being generated via a chemical vapour transport mechanism. As the reaction proceeds, almost the entire silicon surface becomes covered with a 20–100 nm thick polycrystalline nitride scale, while the rest of the product can be observed in the form of needle-like crystals filling the inter-grain space. This needle-like product morphology is considered to be the result of spalling of the product scale from the silicon surface [30].

3. The final overall conversion of silicon and the yield of α-Si_3N_4 increase with an increase in the reaction temperature and/or with a decrease in the nitrogen concentration. The pseudo-asymptotic time dependence of the overall conversion is not clear, but it is suspected that it is related to the presence of coarse grains in the precursor pellets and/or morphology of the product around the silicon grains.

4. Hydrogen concentrations in the range of 5–50 vol% do not significantly affect any of the following: the initial nitridation stage, the final overall conversion, or the yield of the α-form in the product. It only slows the reaction rate in the second stage. However, without hydrogen in the nitriding atmosphere, the reaction is extremely slow.

5. After accounting for some of the structural changes that occur during nitridation, a simple model was derived. The model has shown that the pseudo-asymptotic exponential conversion trend in the second nitridation stage could be explained by various reaction mechanisms adjusted for the spalling of the product scale and properties of the size distribution of silicon grains. After additional simplifications, it is shown that in the investigated range of experimental conditions, nitridation could be considered as having an apparent activation energy of $\approx 340\,\text{kJ}\,\text{mol}^{-1}$.

Acknowledgements

The experimental part of this study was supported by the Division of Chemical and Thermal Systems, National Science Foundation (grants CTS 9241320 and CTS 8921322). The author is grateful to professors Shoichi Kimura and Octave Levenspiel for providing financial support, and their insight along the course of this work. The raw material silicon pellets were prepared and supplied by Shin-Etsu Chemical Company Ltd. The author is particularly grateful to Junichi Koike for providing and interpreting the transmission electron micrographs, and to Nick Wannenmacher for his help in setting-up the experiemental facility.

References

1. F. F. LANGE, *J. Am. Ceram. Soc.* **62** (1979) 428.
2. W. H. RHODES and S. NATANSOHN, *Ceram. Bull.* **68** (1989) 1804.
3. T. YAMADA, *Am. Ceram. Soc. Bull.* **72**(5) (1993) 99.
4. F. K. DIJEN, A. KERBER, U. VOGT, W. PFEIFFER and M. SCHULZE, "Key Engineering Materials 89-91" (Trans. Tech. Publications, Switzerland, 1994) p. 19.
5. DONG-DUK LEE, S. L. KANG, G. PETZOW and D. N. YOON, *J. Am. Ceram. Soc.* **73** (1990) 767.
6. G. HILLINGER and V. HLAVACEK, *Interceram.* **43** (1994) 333.
7. R. A. L. DREW, *Cerâmica* **35** (237) (1989) 129.
8. F. CAMBIER and A. LERICHE, in "The Physics and Chemistry of Carbides; Nitrides and Borides", edited by R. Freer (Kluwer Academic, The Netherlands, 1990) pp. 13–28.
9. D. GELDART, *Chem. Eng. Sci.* **39** (1984) 1481.
10. D. KUNII and O. LEVENSPIEL, "Fluidization Engineering", 2nd Edn (Butterworth–Heinemann, Boston, 1991).
11. M. SHIMIZU, European Pat. Applic. no. 90 114 382.6 (1991).
12. M. SHIMIZU, H. FUKUOKA and M. FUKUHIRA, US Pat. no. 5073 385 (1991).
13. H. FUKUOKA, M. SHIMIZU, H. OCHIAI, H. SHIMIZU and M. FUKUHIRA, US Pat. no. 5232 677 (1993).
14. P. E. D. MORGAN, *J. Mater. Sci.* **15** (1980) 791.
15. M. BARSOUM, P. KANGUTKAR and M. J. KOCZAK, *J. Am. Ceram. Soc.* **74** (1991) 1248.
16. R. G. PIGEON, A. VARMA and A. E. MILLER, *J. Mater. Sci.* **28** (1993) 1919.
17. M. W. LINDLEY, D. P. ELIAS, B. F. JONES and K. C. PITMAN, *ibid.* **14** (1979) 70.
18. H. DERVISBEGOVIC and F. L. RILEY, *ibid.* **16** (1981) 1945.
19. W. M. DAWSON and A. J. MOULSON, *ibid.* **13** (1978) 2289.
20. T. ITOH, *J. Mater. Sci. Lett.* **10** (1991) 19.
21. H. M. JENNINGS, *J. Mater. Sci.* **18** (1983) 951.
22. Z. R. JOVANOVICS, S. KIMURA and O. LEVENSPIEL, *J. Am. Ceram. Soc.* **77** (1994) 186.
23. D. CAMPOS-LORIZ and F. L. RILEY, *J. Mater. Sic.* **13** (1978) 1125.
24. A. ATKINSON, A. J. MOULSON and E. W. ROBERTS, *J. Am. Ceram. Soc.* **59** (1976) 285.
25. H. DERVISBEGOVIC and F. L. RILEY, *J. Mater. Sci.* **14** (1979) 1265.
26. H. M. JENNINGS, B. J. DAGLEISH and P. L. PRATT, *ibid.* **23** (1988) 2573.
27. D. S. THOMPSON and P. L. PRATT, in "Science of Ceramics", Vol. 3, edited by G. H. Stewart (Academic Press, New York, 1967) p. 33.
28. Y. INOMATA, *J. Ceram. Soc. Jpn* **83** (1975) 497.
29. Y. INOMATA and Y. UEMURA, *ibid.* **83** (1975) 244.
30. J. KOIKE and S. KIMURA, *J. Am. Ceram. Soc.* **79** (1996) 365.
31. M. N. RAHAMAN and A. J. MOULSON, *J. Mater. Sci.* **19** (1984) 189.
32. B. MYHRE and K. MOTZFELDT, in "The Physics and Chemistry of Carbides; Nitrides and Borides", edited by R. Freer (Kluwer Academic, The Netherlands, 1990) p. 29.
33. B. W. SHELDON. J. SZEKELY and J. S. HAGERTY, *J. Am. Ceram. Soc.* **75** (1992) 677.
34. Y. D. LIU and S. KIMURA, *Powder Technol.* **75** (1993) 189.
35. Z. R. JOVANOVIC, PhD dissertation, Oregon State University, Corvallis, OR, USA (1994).
36. Z. R. JOVANOVIC and S. KIMURA, *J. Am. Ceram. Soc.* **77** (1994) 2226.
37. R. G. PIGEON and A. VARMA, *J. Mater. Sci.* **28** (1993) 2999.
38. W. KU, O. GREGORY and H. M. JENNINGS, *J. Am. Ceram. Soc.* **73** (1990) 286.
39. J. SZEKELY, J. W. EVANS and H. Y. SOHN, "Gas-Solid Reactions" (Academic Press, New York, 1976).
40. J. HEINRICH, *Eur. Space Agency Report* no. N-81-22113, December 1990.

41. N. J. SHAW and F. J. ZELEZNIK, *Commun. Am. Ceram. Soc.* **65** (1982) C-180.
42. J. HEINRICH and G. STREB, *J. Mater. Sci.* **14** (1979) 2083.
43. S. KIMURA, *personal communication*, Chemical Engineering Department, Oregon State University, Corvallis, OR 97331, USA (1995).
44. I. J. R. BAUMVOL, F. C. STEDILE, J. J. GANEM, S. RIGO and I. TRIMAILLE, *J. Electrochem. Soc.* **142** (1995) 1205.
45. K. KIJIMA, and S. SHIRSAKI, *J. Chem. Phys.* **65** (1976) 2668.
46. J. W. CHRISTIAN, in "The Theory of Transformations in Metals and Alloys; Part I-Equilibrium and General Kinetic Theory", 2nd Edn (Pergamon Press, Oxford, 1975) pp. 410–17.
47. R. M. BARRER, "Diffusion in and through Solids" (Cambridge University Press, Cambridge, 1951).
48. S. M. SZE, "Physics of Semiconductor Devices" (Wiley, New York, 1981).
49. A. F. WELLS, "Structural Inorganic Chemistry", 3rd Edn (Oxford University Press, New York, 1962).
50. A. T. FROMHOLD Jr, in "Defects in Crystalline Solids: Fundamentals", Vol. 9, edited by S. Amelinckx, R. Gevers and J. Nihoul (North-Holland, Amsterdam, New York, Oxford, 1976) p. 28.
51. Y. HAYAFUJI and K. KAJIWARA, *J. Electrochem. Soc. Solid State Sci. Technol.* **129** (1982) 2102.
52. O. KUBASCHEWSKI and B. E. HOPKINS, "Oxidation of Metals and Alloys", 2nd Edn (Butterworths, London, 1962).
53. M. I. MENDELSON, *J. Mater. Sci.* **14** (1979) 1752.
54. H. M. JENNINGS and M. H. RICHMAN, *ibid.* **11** (1976) 2087.
55. U. R. EVANS, "The Corrosion and Oxidation of Metals: Scientific Principles and Practical Applications" (Edward Arnold, London, 1967).
56. G. A. ROSSETTI Jr and R. P. DENKEWICZ Jr, *J. Mater. Sci.* **24** (1989) 3081.
57. S. YAGI and D. KUNII, in "Proceedings of the Fifth International Symposium on Combustion (1955)" (Van Nostrand Reinhold, New York, 1955) p. 231.
58. G. VALENSI, *Comput. Rend.* **202** (1936) 309.
59. R. E. CARTER, *J. Chem. Phys.* **34** (1961) 2010.
60. Z. R. JOVANOVIC, *J. Mater. Sci. Lett.* **14** (1995) 1263.
61. PSI-PLOT, "Technical Plotting and Data Processing" (Poly Software International Ltd, Salt Lake City, 1993).
62. O. LEVENSPIEL, "The Chemical Reactor Omnibook" (OSU Book Stores, Corvallis, OR 97331, 1993).
63. S. KIMURA, Y. TAKAGI, S. TONE and T. OTAKE, *J. Chem. Eng. Jpn* **16** (3) (1983) 217.

Received 27 March
and accepted 17 December 1997